

The Direct Conversion of Heat to Electricity Using Multiferroic Alloys

Vijay Srivastava, Yintao Song, Kanwal Bhatti, and R. D. James*

We demonstrate a new method for the direct conversion of heat to electricity using the recently discovered multiferroic alloy, $\text{Ni}_{45}\text{Co}_5\text{Mn}_{40}\text{Sn}_{10}$ ^[1]. This alloy undergoes a low hysteresis, reversible martensitic phase transformation from a nonmagnetic martensite phase to a strongly ferromagnetic austenite phase upon heating. When biased by a suitably placed permanent magnet, heating through the phase transformation causes a sudden increase of the magnetic moment to a large value. As a consequence of Faraday's law of induction, this drives a current in a surrounding circuit. Theory predicts that under optimal conditions the performance compares favorably with the best thermoelectrics. Because of the low hysteresis of the alloy, a promising area of application of this concept appears to be energy conversion at small ΔT , suggesting a possible route to the conversion of the vast amounts of energy stored on earth at small temperature difference. We postulate other new methods for the direct conversion of heat to electricity suggested by the underlying theory.

Fundamentally, this is owing to the absence of diffusion and other relaxation processes and the presence of a low energy mode of transformation between crystalline lattices, i.e., the passage of many austenite-martensite interfaces. Martensitic transformations are typically quite fast, with speeds of interfaces an appreciable fraction of the speed of sound in the material.^[12] With a large change in the lattice parameters, large free energy changes are typical. Partly for these reasons, the highest energy density actuator, that converts heat to mechanical work, is the shape memory alloy NiTi,^[13] which undergoes a reversible martensitic transformation from a cubic to a monoclinic phase. Numerous emerging devices convert mechanical vibrations into electricity using piezoelectric, ferroelectric, magnetostrictive or ferromagnetic shape memory effects. These rely on quite different physical

processes so we do not review them here.

With its low hysteresis and its large and abrupt change in magnetization at transformation, we conjecture that the natural application area for our device is energy conversion at small temperature difference. Cyclic heat engines of this type are necessarily of low efficiency, because the efficiency of all such devices is bounded by the Carnot efficiency $1 - T_{\min}/T_{\max}$, T_{\min} (resp., T_{\max}) being the lowest (resp., highest) temperature experienced by any part of the device during the cycle, according to a fundamental theorem of thermodynamics. However, the definition of efficiency, $\eta = (\text{net work done})/(\text{total heat absorbed})$ during the cycle, expressed in purely economic terms, is typically (energy sold)/(fuel bought). Given that all internal combustion engines waste heat at small temperature difference through cooling, it may be that the standard definition of efficiency is irrelevant. More generally, there are enormous reserves of energy on earth stored at small temperature difference, notably, the $\sim 20^\circ\text{C}$ difference between surface ocean temperatures and temperatures just below the thermocline in mid-latitude waters. What is needed in such cases is a more suitable measure of efficiency, consistent with thermodynamics at small temperature difference.

Multiferroic alloys that could be utilized in energy conversion devices must have highly reversible phase transformations.^[14] A change of lattice parameters typically implies the presence of stress, notably in the transition layer between phases at the austenite/martensite interface.^[15] If this stress is sufficiently large, it can drive the formation of dislocations and other defects that, after sufficiently many cycles of transformation, may lead to widening thermal hysteresis, migration of transformation

1. Introduction

While the goal of discovering a material that is both strongly ferroelectric and strongly ferromagnetic remains elusive, numerous other interesting multiferroic materials are emerging.^[1–9] A particularly fertile area for discovery are crystalline materials having a big first order phase transformation, but with no diffusion.^[10] Multiferroic properties like polarization or magnetization are generally sensitive to changes of lattice parameters.^[2,8,11] In a material that undergoes a phase transformation having an abrupt change of lattice parameters, one can expect the two phases to exhibit diverse electromagnetic properties. The alloy $\text{Ni}_{45}\text{Co}_5\text{Mn}_{40}\text{Sn}_{10}$, that is used in energy conversion device described here, is of this type. It has a strongly ferromagnetic austenite phase, with magnetization approaching that of iron, and a nonferromagnetic martensite phase.

Alloys that undergo such martensitic phase transformations are also attractive for energy storage and conversion.

Dr. V. Srivastava, Y. Song, Dr. K. Bhatti, Dr. R. D. James
Department of Aerospace Engineering and Mechanics
University of Minnesota
Minneapolis, MN 55455, USA
E-mail: james@umn.edu

Dr. K. Bhatti
Department of Chemical Engineering and Materials Science
University of Minnesota
Minneapolis, MN 55455, USA

DOI: 10.1002/aenm.201000048

temperatures, or failure.^[16–18] At a macroscopic level such processes are often seen as the competition between phase transformation and crystal plasticity.

The particular alloy $\text{Ni}_{45}\text{Co}_5\text{Mn}_{40}\text{Sn}_{10}$ used here was found by implementing a new strategy for improving the reversibility of phase transformations. This can be expressed^[11,15,19] as the condition $\lambda_2 = 1$, where λ_2 is the middle eigenvalue of the transformation stretch matrix. When $\lambda_2 = 1$, the stressed transition layer in the austenite/martensite interface disappears.^[20] In recent alloy development programs done by combinatorial synthesis methods,^[21,22] the thermal hysteresis of phase transformations in NiTiX ($X = \text{Pd}, \text{Pt}, \text{Au}$) has been shown to drop precipitously from more than 30° to less than 6 °C as $\lambda_2 \rightarrow 1$. A particularly dramatic example of Zarnetta et al.^[22] in NiTiCuPd alloys shows a hysteresis near zero^[23] and corresponding improvement of the reversibility of transformation, quantified by the migration of hysteresis loops under repeated transformation, as $\lambda_2 \rightarrow 1$. The alloy $\text{Ni}_{45}\text{Co}_5\text{Mn}_{40}\text{Sn}_{10}$ ($\lambda_2 = 1.0032$) used here was discovered by this kind of tuning of lattice parameters by systematic change of composition.^[1] Having $\lambda_2 = 1$ does not contradict an otherwise large change of lattice parameters, i.e., the other eigenvalues of the stretch matrix can remain far from 1, so the aforementioned abrupt change of electromagnetic properties is possible. In this general alloy system we found a correlation between the large magnetization of austenite and

λ_2 , with the maximum magnetization occurring near $\lambda_2 = 1$. An understanding of the the origins of this correlation is currently unavailable.

2. Characterization of $\text{Ni}_{45}\text{Co}_5\text{Mn}_{40}\text{Sn}_{10}$ for Energy Conversion

The particular properties of this alloy $\text{Ni}_{45}\text{Co}_5\text{Mn}_{40}\text{Sn}_{10}$ influenced the design of the demonstration. **Figure 1** shows the magnetization vs. temperature measured in this alloy. At the applied field of 1 T the phase transformation on heating causes an increase of the magnetization from less than 10 emu/cm^3 in the martensite phase to more than 1100 emu/cm^3 in the austenite phase. The austenite is nevertheless magnetically very soft with a susceptibility of $\chi_a = 2.3 \text{ emu}/\text{cm}^3\text{Oe}$ measured from the data of Figure 1d near $H = 0$. Magnetization vs. temperature at 0.5 T is nearly the same as shown in Figure 1a. Figure 1c suggests an inhomogeneous structure containing a small volume fraction of ferromagnetic particles in an antiferromagnetic matrix. Notice that this high magnetization of austenite occurs even though the transformation temperature $\theta_c = (A_s + M_f)/2$ measured^[23] at low field is quite close to the approximate Curie temperature of 167 °C. These temperatures are somewhat high for the design of actual devices, but in this family of alloys, and in martensitic

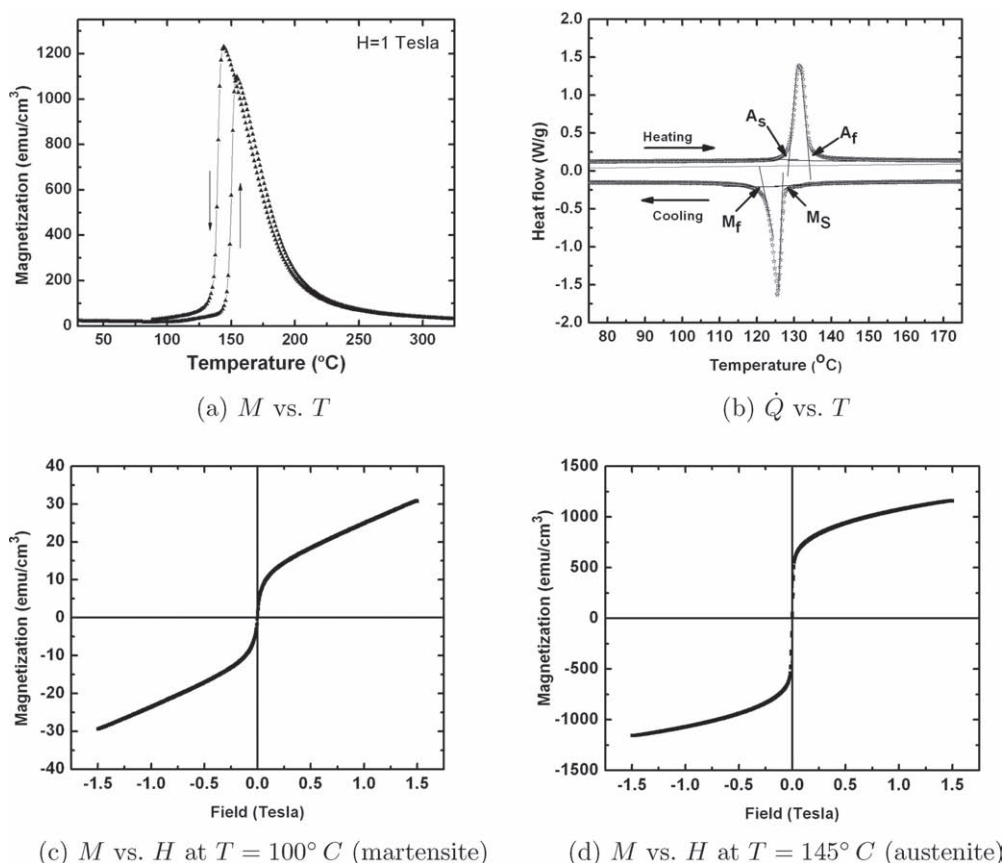


Figure 1. Relevant properties of $\text{Ni}_{45}\text{Co}_5\text{Mn}_{40}\text{Sn}_{10}$. a) Magnetization vs. temperature under 1 T field. b) Heat flow vs. temperature. Magnetization vs. applied field in martensite (c) and in austenite (d) (Note the different scales). Reproduced with permission.^[1] Copyright 2010, American Institute of Physics.

transformations in general, transformation temperatures are extremely sensitive to composition. Further alloy development would be needed to tune both λ_2 and θ_c . The thermal hysteresis measured by calorimetry (Figure 1b) is $A_s - M_f = 6^\circ\text{C}$ and the latent heat is 16.5 J/g. The magnetization curves show zero remanence and coercivity within experimental error. This implies that changes of magnetization contributed negligible loss to the device. This also necessitated the use of a permanent magnet to bias the material, so that, upon heating to austenite, a uniformly magnetized sample was achieved. The loss due to the phase transformation is indicated by the hysteresis loops in several of the measurements.

3. Energy Conversion Device and Voltage Measurements

We show a schematic view of our demonstration in Figure 2. The specimen is fixed (to prevent movement) near a pole of a permanent bar magnet and is surrounded by a coil. Heat is supplied by an external heat gun. The basic idea is that, upon transformation on heating, the average magnetization \mathbf{M} is increased in the specimen, giving a substantial component of $d\mathbf{M}/dt$. Demagnetization is prevented by the presence of the nearby permanent magnet. The fundamental dipolar relationship between the magnetization \mathbf{M} , the magnetic induction \mathbf{B} and magnetic field \mathbf{H} ,

$$\mathbf{B} = \mathbf{H} + 4\pi\mathbf{M}, \quad (1)$$

then gives a nonzero $d\mathbf{B}/dt$. The precise way in which the magnetization is partitioned between \mathbf{H} and \mathbf{B} is governed by micromagnetic considerations. A consequence of the design is that $d\mathbf{B}/dt \neq 0$ is induced in by the phase transformation. According to Faraday's law

$$\text{curl}\mathbf{E} = \frac{-1}{c} \frac{d\mathbf{B}}{dt}, \quad (2)$$

an electric field is created during transformation. The design of the coil is to give a maximal component of \mathbf{E} parallel to the wire, thereby driving a current. A potential difference across the coil of opposite polarity is obtained on the reverse phase transformation upon cooling.

Besides the micromagnetic considerations mentioned above, this analysis is too simple in another respect. The current created in the coil itself places a back field on the material, decreasing the overall rate of change of \mathbf{B} . A more accurate analysis accounting for this effect leads to a differential equation for the current described below.

We show a picture of the actual device in Figure 2b. The specimen of $\text{Ni}_{45}\text{Co}_5\text{Mn}_{40}\text{Sn}_{10}$ was arc-melted from elemental materials and, to retain as much mass as possible, it was not cut down to a convenient shape. The surrounding coil consisted of 2000 turns of fine insulated copper wire. A large resistance of $10\text{ k}\Omega$, placed between the ends of the coil, gave a potential difference between its ends during heating. Figure 3 shows the potential difference across the coil vs. time, and the temperature vs. time (inset of 3b), measured simultaneously upon heating. The temperature measurement was done with a thermocouple placed below the specimen and therefore must be considered an approximate representation of the temperature field on the specimen. The measured temperature vs. time is approximately monotone, so in Figure 3b we eliminate time between these plots and get the graph of voltage vs. temperature. We interpret the plateau in the inset as being due the absorption of latent heat: the lack of strict monotonicity here causes a slight reversal on voltage vs. temperature. By comparison with magnetization vs. temperature shown in Figure 1a, we interpret the first rapid rise as due to the phase transformation. We interpret the subsequent sharp decrease as due to the rapid fall of magnetization vs. temperature close to the Curie temperature, as seen in Figure 1a. The cooling curves confirm this interpretation.

We have written down Faraday's law in a form appropriate to the assumed geometry, including the back field of the induced current. The details will be presented elsewhere.^[24] We treat the shape effect using an axial demagnetization factor $0 \leq \delta \leq 4\pi$. For an assumed time-dependent susceptibility $\chi(t)$ we get the following differential equation for the current induced in the coil:

$$\begin{aligned} & \left(\frac{4\pi AN(1 + (4\pi - \delta)\chi(t))}{c^2 L_{\text{eff}}} \right) I'(t) \\ & + \left(\frac{8r_c}{d^2\sigma} + \frac{R}{N} + \frac{4\pi AN(4\pi - \delta)\chi'(t)}{c^2 L_{\text{eff}}} \right) I(t) \\ & + \frac{A(4\pi - \delta)\chi'(t)h_0}{c} = 0. \end{aligned} \quad (3)$$

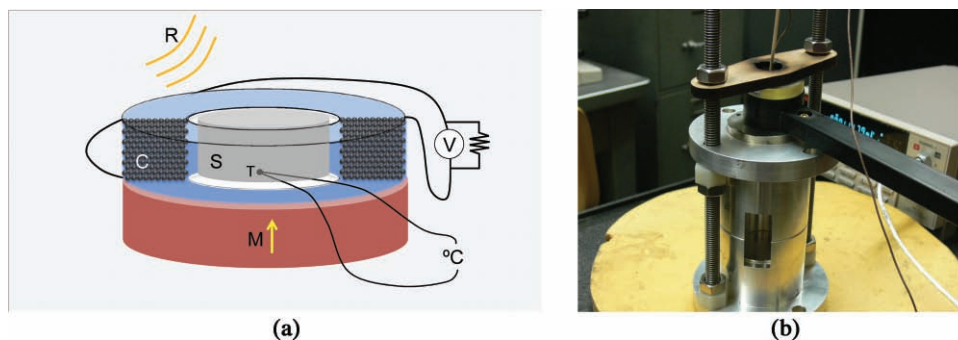


Figure 2. Schematic (a) and actual (b) views of the demonstration. C, coil; R, heat source; S, specimen of $\text{Ni}_{45}\text{Co}_5\text{Mn}_{40}\text{Sn}_{10}$; M, permanent magnet with direction of magnetization indicated; T, thermocouple; V, voltmeter.

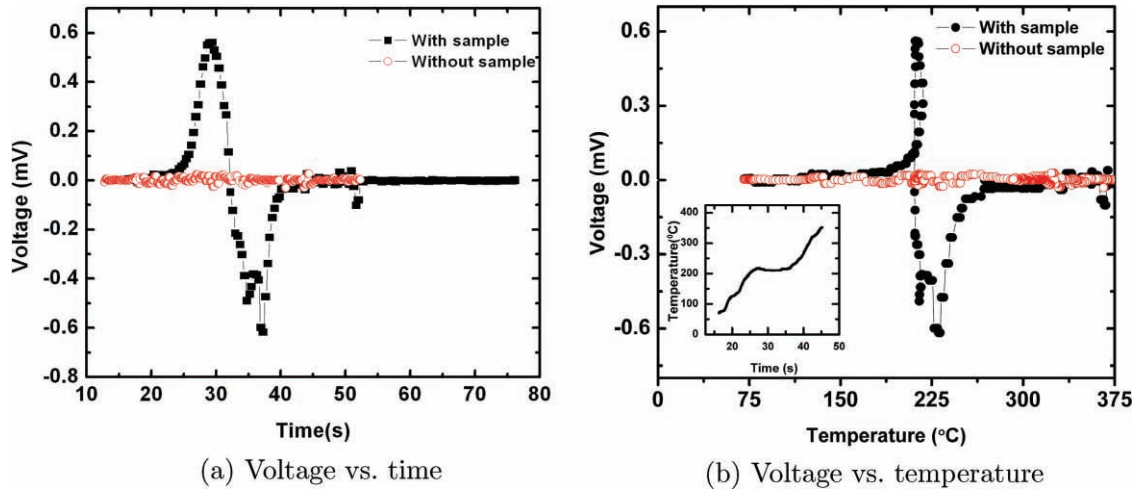


Figure 3. Measurements of a) voltage vs. time, and b) voltage vs. temperature. The graph (b) is obtained from (a) by elimination of the time using the inset. The open circles give the corresponding measurements done with the specimen absent.

Here, $A = \pi D^2/4$ is the cross-sectional area of the specimen and the other quantities are defined in **Table 1**. L_{eff} is given by a standard formula for the effective length of the coil of inner/outer radii r_1, r_2 and length L , accounting for flux leakage at the end:

$$L_{\text{eff}} = 2(r_2 - r_1) / \ln \left(\frac{2r_2 + \sqrt{L^2 + 4r_2^2}}{2r_1 + \sqrt{L^2 + 4r_1^2}} \right). \quad (4)$$

In the special case of a susceptibility that is linear in time,

$$\chi(t) = (t/t_1)\chi_a + ((t_1 - t)/t_1)\chi_m, \quad (5)$$

Table 1. Values of parameters used in the evaluation.

Parameter	Description	Value	Unit
c	speed of light	3×10^{10}	cm s^{-1}
D	diameter of the specimen	0.75	cm
δ	demagnetization factor	2.5π	
N	number of turns in the coil	2000	
r_1	inside radius of the coil	0.95	cm
r_2	outside radius of the coil	1.9	cm
r_c	average radius of the coil	1.425	cm
L	length of the coil	0.8	cm
d	diameter of the wire	0.013	cm
σ	electrical conductivity of the wire (Cu)	5.4×10^{17}	s^{-1}
R	external resistance	$10 \text{ k ohm} = 10^{13}/c^2$	s cm^{-1}
h_0	magnitude of the applied magnetic field	2000	Oe
χ_a	average susceptibility of the austenite	0.1	$\text{emu cm}^{-3}\text{Oe}^{-1}$
Q_1	latent heat of the specimen	13.2×10^8	erg cm^{-3}
t_1	transformation time	10	s

(3) becomes

$$(C_1 t + C_2)I'(t) + C_3 I(t) + C_4 = 0, \quad (6)$$

where

$$\begin{aligned} C_1 &= \frac{4\pi AN(4\pi - \delta)(\chi_a - \chi_m)}{c^2 t_1 L_{\text{eff}}}, \\ C_2 &= \frac{4\pi AN(1 + (4\pi - \delta)\chi_m)}{c^2 L_{\text{eff}}}, \\ C_3 &= \frac{8r_c}{\sigma d^2} + \frac{R}{N} + \frac{4\pi(4\pi - \delta)AN(\chi_a - \chi_m)}{c^2 t_1 L_{\text{eff}}}, \\ C_4 &= \frac{(4\pi - \delta)A(\chi_a - \chi_m)h_0}{c t_1}, \end{aligned} \quad (7)$$

Here, χ_m is the susceptibility of martensite. The special case (6) is particularly useful for parameter studies because the solution can be written down explicitly. The general solution of (6) is

$$I(t) = \left(I_0 + \frac{C_4}{C_3} \right) \left(1 + \frac{C_1}{C_2} t \right)^{-\frac{C_3}{C_1}} - \frac{C_4}{C_3} \quad (8)$$

This solution has a short-lived transient followed by saturation to the value $I(t) \approx -C_4/C_3$. This current gives a constant back field that opposes the field due to the permanent magnet. Rapid heating through the phase transformation strongly favors a big back field, and, together with the large magnetization, gives a higher work output.

4. Comparison Between Theory and Experiment and Optimization

In this section we give two kinds of predictions of the model. In the first comparison we use the actual parameters estimated from the experiment. We also examine the effect of certain minor changes of the experiment that can lead to improvements. In the second comparison we seek a geometry and

parameter regime that is expected to be realizable, and which leads to substantial improvements. We call the latter an optimized demonstration.

The parameters corresponding to the actual demonstration are given in Table 1. Most of values are accurately known or straightforward to estimate. There is difficulty with h_0 , because the precise location of the specimen while heating was not known. But the main difficulty is χ_a , because the specimen contained a temperature gradient while being heated and therefore experienced a range of susceptibilities (cf., Figure 1a) at any given time. The value $\chi_a = 0.1$ was obtained by averaging the graph of Figure 1a over an estimated temperature interval. The value of $\chi_m \ll \chi_a$ is taken to be 0. The value of the demagnetization factor was also approximate, since the shape of the active volume was not known (The specimen contained several cracks.) The time t_1 is taken to be the approximate duration of the first peak in Figure 3a. The applied field was measured directly in the device with the specimen absent, and Q_e is measured directly from the area under the curve in Figure 1b. With these values the transient term in (8) decays very quickly in a small fraction of t_1 . Inserting these values into (8) and multiplying by R we predict an output voltage of 0.81 mV. The measured peak voltage is about 0.6 mV (cf., Figure 3a).

To give a more realistic description of the transformation process, we now use a time-dependent $\chi(t)$ but leave the rest of the Table 1 the same. Referring to Figure 4, we now discard the assumption (5) and use (3), choosing $\chi(t)$ that gives an approximate representation of the variation of susceptibility during the full heating cycle seen in Figure 3a. This can only be done semi-quantitatively, because some details (precise shape, thermal conductivity) needed for the heat transfer problem are inexactly known and the kinetics of this phase transformation is completely unknown. In this case the solution (8) is no longer valid, and we did a direct numerical integration of (6) with the time-dependent $\chi(t)$ shown in Figure 4a. The result is seen in Figure 4b. This shows qualitative agreement with Figure 3a. As above, the peak values are a little overestimated: this is likely due to overestimation^[25] of the active volume of the specimen.

Better performance would be expected with a specimen that fills the region inside the coil. If we fill the volume inside

the coil with the specimen ($D = 1.9$ cm), use an appropriate demagnetization factor ($\delta = 6.4$, based on the aspect ratio of 1.9/1 of the coil used) and use the peak susceptibility measured above ($\chi_a = 2.3$ emu/cm³Oe), leaving the other values in Table 1 the same, we predict a voltage several orders of magnitude bigger, 156 mV.

Now we use our measured properties of Ni₄₅Co₅Mn₄₀Sn₁₀ but consider the effect of optimizing the geometry and external resistance. Further improvements are expected by taking advantage of the natural scaling of (8). The role of L_{eff} in (8) suggests that platelike specimens are advantageous. The scaling of the heat equation is such that if the specimen thickness is scaled by k , then the time for the center of the plate to change temperature by a fixed amount is scaled by k^2 . Assuming again that the specimen fills the region inside the coil, we replace L by L/k in the formula for L_{eff} and t_1 by t_1/k^2 in (8), and we examine what happens when k is increased. Since this also changes the volume of the specimen, we divide by the volume in comparisons below.

This scaling also however affects other material constants in Table 1. In particular, we replace N by N/k to ensure that the coil always has the length of the specimen. In addition, demagnetization factors degrade as the specimen gets thinner. For this we use the standard formula (see ref. [26], eq. (2.24)) for the demagnetization factor of an oblate ellipsoid with aspect ratio k ,

$$\delta = \frac{4\pi k^2}{k^2 - 1} \left(1 - \sqrt{\frac{1}{k^2 - 1}} \arcsin \frac{\sqrt{k^2 - 1}}{k} \right). \quad (9)$$

At $k = 1$, $\delta = 4\pi/3$ (sphere) and $\delta \rightarrow 4\pi$ as $k \rightarrow \infty$ (i.e., the standard formula for a thin plate). We also choose an optimized external resistance. Except where noted, we choose the external resistance R to be the unique value that maximizes the power output for each choice of parameters given below.

Modest increases in k (thinner plate, shorter heating time) have a big effect on voltage and power density. For example, if we begin with the constants for the improved experiment above (Table 1, but with $D = 1.9$ cm, $\chi_a = 2.3$ emu/cm³Oe, and L, t_1, δ scaled with k as described above) we find that the power density increases rapidly with k , then linearly. At the modest value $k = 50$ we already have a power density

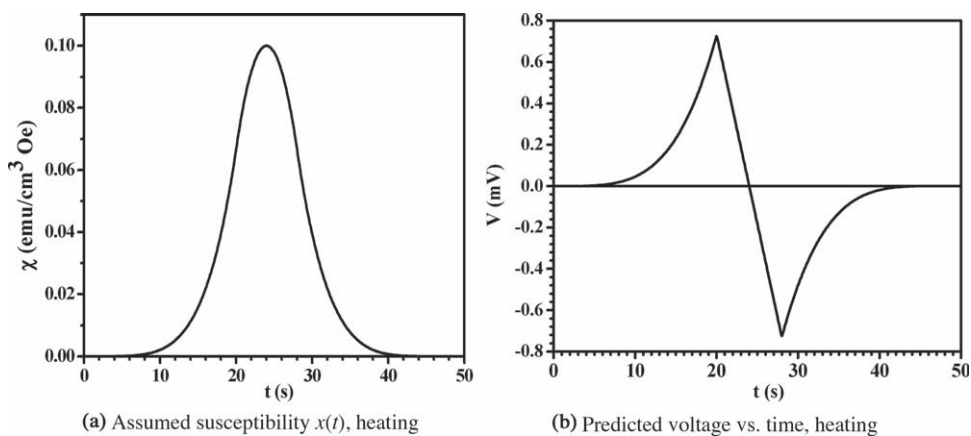


Figure 4. Numerical solution of (3) with assumed susceptibility $\chi(t)$ modeling the demonstration.

of 3.1×10^6 erg/cm³s, an energy density per (half) cycle of 1.2×10^4 erg/cm³, and a predicted voltage of 502 mV with $R = 10$ kohm. Greater improvements (per volume) are suggested for thin films with patterned coils.

The behavior of demagnetization factors with k given in (9) suggests another interesting scaling. The demagnetization factor behaves much better for a thin rod, while the advantages of the thermal scaling persist. But the design of the experiment has to change to permit the rapid heating of one or more rods. We consider several alternatives below, in which k is now the aspect ratio (length/diameter) of the rod:

- (1) Thin rods with a tightly wound coil of one layer deployed on a surface. This is intended to allow rapid heating and to accommodate a flux path below the surface. We now let $k = L/D$ be the aspect ratio, so again we are interested in large values of k . In this case, to a very good approximation for $k > 10$ (particularly with a flux path), $\delta = 0$. Also, for a single layer coil we have $(r_2 - r_1)/L \ll 1$ in the formula for L_{eff} in which case $L_{\text{eff}} \approx L$. Other constants are modified as follows: $L \rightarrow L$, $D \rightarrow 1.9/k$, $N \rightarrow L/d$, $r_1 \rightarrow 0.95/k$, $r_2 \rightarrow 0.95/k + d$, $r_c \rightarrow 0.95/k + d/2$, $\chi_a \rightarrow 2.3$ (peak susceptibility), $t_1 \rightarrow 10/k^2$. In this case again the power density increases rapidly with k and then linearly, while the energy density per (half) cycle saturates, but more slowly than in the case of a thin plate. At $k = 500$ the power density is 6.8×10^8 erg/cm³s and the energy density per (half) cycle is 2.7×10^4 erg/cm³. This high power density is only produced at a voltage of 5 mV.
- (2) Hollow rods, or rods separated from the coil by a small space, heated/cooled by a flowing fluid. We now envision a long thin specimen ($\delta = 0$, $L_{\text{eff}} = L$) but heated/cooled through its hollow core, or between itself and the coil. Obviously, the temperature changes cannot be as rapid in this case (in practice, k is limited). With the constants and scaling of the preceding item except with $N = 1000$, the power and energy densities are similar to those in Item 1, but this is produced at the higher voltage of 82 mV.

5. Comparison with Thermoelectric Materials

It is illustrative to compare our results with the most promising other device for the direct conversion of heat to electricity, thermoelectrics.^[27] As explained below, even an optimized version of our demonstration has low efficiency. However, the predicted voltage output for an optimized device is comparable to that of good thermoelectric materials. The predicted power density of an optimized device is more than an order of magnitude greater than thermoelectrics with the highest known ZT value. Our predictions involve optimizing the geometry, but otherwise only use the measured data of Ni₄₅Co₅Mn₄₀Sn₁₀ shown in Figure 1.

The thermoelectric effect refers to the direct production of electricity from a temperature gradient using the Seebeck effect, and its converse. Normally thermoelectrics use a larger temperature difference than that for which the present demonstration seems best suited. However, thermoelectrics and

our demonstration are both capable of converting heat to electricity with no moving parts, and it is natural to compare them. It should be born in mind that the Seebeck effect was discovered in 1821, and thermoelectrics have been the subject of intense study and optimization, especially during the past 53 years.

In all the comparisons below we use the temperature interval of 10 °C which includes the support of the first peak in Figure 3b, which has been interpreted as the phase transformation.

We re-emphasize that the present materials seem best suited to conversion of energy at small temperature difference in which efficiency may not be the best measure of performance. Nevertheless, this measure is often applied to thermoelectrics. The efficiency of thermoelectric materials is measured by zT where $z = \sigma S^2/\kappa$, σ is electrical conductivity, κ is thermal conductivity, and S is the temperature dependent Seebeck coefficient. Peak values of zT for the the material of best thermoelectric devices is near 1. The whole device efficiency is often measured by ZT , also of order 1 in the best devices,^[28] and the efficiency is given by

$$\eta = \frac{(\sqrt{1+ZT} - 1)\Delta T}{(\sqrt{1+ZT} + 1)T_{\text{max}} - \Delta T} \approx \frac{\sqrt{2} - 1}{\sqrt{2} + 1} \frac{\Delta T}{T_{\text{max}}} \quad (10)$$

where ΔT and T_{max} are the temperature difference and maximum temperature in a thermal cycle of the device.^[27] With $\Delta T = 10$ K, $ZT = 1$, and $T = 300$ K, we get an efficiency of 0.57%. If we consider our optimized demonstration of the preceding section, we have an energy density per cycle of 5.4×10^4 erg/cm³. As a reasonable estimate of the heat added we take the latent heat, measured to be 13.2×10^8 erg/cm³. This gives a rather low efficiency of 0.004%. In our present designs a lot of the latent heat is not being used to make electricity.

Other measures of performance are more favorable. The voltage output of of a thermoelectric material is given directly by its Seebeck coefficient. The thermoelectric material Bi₂Te₃ has a large Seebeck coefficient of $-230 \mu\text{V/K}$. The standard thermocouple with the highest Seebeck coefficient is Chromel-Constantan at $60 \mu\text{V/K}$. At $\Delta T = 10$ K these values give respectively 2.3 mV and 0.6 mV. We have measured 0.6 mV in our device. Under reasonable hypotheses in an optimized device we predict 502 mV. Thermoelectric devices arrange many individual thermoelectric elements in series to boost the voltage. Apparently, we could do the same, so we have compared only materials.

An important comparison is power density. A commercial thermoelectric generator (TG12-8, Marlow Industries^[29]) has $ZT = 0.73$ and a power density at $110 - 50 = 60$ °C of 1.83×10^6 erg/cm³s. Scaling this to 10 °C gives a power density of 3.05×10^5 erg/cm³s. A recent high power thermoelectric device^[28] exhibited a measured $250 \text{ W}/\ell = 2.5 \times 10^6$ erg/cm³s power density (not including fluid manifolds), achieved at a temperature difference of 180 °C. Scaling proportionately to 10 °C, this is 1.4×10^5 erg/cm³s. Our predicted values of 3.1×10^6 erg/cm³s for a thin plate and 6.8×10^8 erg/cm³s for a thin rod (excluding the coil and permanent magnet in both cases) compare favorably.

Table 2. Methods of conversion of heat to electricity using phase transformations in multiferroics. In all cases the transformation is induced by direct heating and cooling. M_s is the saturation magnetization. P_s the saturation polarization, and T_c the Curie temperature (magnetic or ferroelectric, resp.).

	Phase 1	Phase 2	Physics	Notes
1.	Ferromagnetic	Nonmagnetic	Faraday's law	Biasing by a permanent magnet; external coil
2.	Ferroelectric	Nonferroelectric	Ohm's law	Biasing by a capacitor; polarization-induced current
3.	Ferromagnetic; high anisotropy	Ferromagnetic; low anisotropy	Faraday's law	Biasing by a permanent magnet, intermediate magnetic field; external coil
4.	Ferroelectric; high permittivity	Ferroelectric; low permittivity	Ohm's law	Biasing by a capacitor, intermediate electric field; polarization-induced current
5.	Ferroelectric; large P_s near T_c (large pyroelectric coefficient)	Nonpolar	Ohm's law	Second-order transition; biasing by a capacitor
6.	Ferromagnetic; large M_s near T_c (small critical exponent)	Nonmagnetic	Faraday's law	Second-order transition; biasing by a permanent magnet ^[31]
7.	Nonpolar; nonmagnetic	Nonpolar; nonmagnetic	Stress-induced transformation; Faraday's law	Shape-memory engine driving generator; biased by stress ^[32]

6. Related Methods of Conversion of Heat to Electricity using Multiferroic Materials

The device presented here represents one of several ways multiferroics can be used as new kinds of energy conversion devices. For the purpose of this report we confine attention to what appear to be the most promising: devices that convert heat directly to electricity, realized, say, as current flow through a resistor, and that involve a phase transformation without diffusion.

We present a summary in Table 2. To our knowledge, only rows 6 and 7 have been previously realized. Although the design of the device would be affected, it is otherwise unimportant whether phase 1 is the high temperature or low temperature phase. For all these cases one must pay due attention to reversibility and low hysteresis, so these terms are omitted from the last column. Some of these cases are obvious. Others are more subtle. While the present alloy uses a big difference in magnetization of the two phases, this is not essential. One could have a transformation between phases having nearly the same magnetization, but quite different magnetic anisotropy, as in the prototype alloy Ni_2MnGa .^[30] In that case a carefully tuned applied field would easily rotate the magnetization in one phase (austenite, in Ni_2MnGa) but not in the other, leading to an effective large change of the magnetic moment during transformation. Ferroelectrics can be used like ferromagnetics in many ways, Table 2, but have the additional flexibility of being able to directly move free charges. An interesting possibility revealed by the presence of the second peak Figure 3a is that the quite sharp drop at the Curie temperature can also induce a significant voltage. In fact, this possibility was noticed long ago by Tesla.^[31] We have concentrated on simple mechanisms in Table 2. Given a suitable material exhibiting two or more effects, more sophisticated devices are possible.

7. Experimental Section

The active material for both the property measurements and the demonstration was obtained from a polycrystalline button (3β) of

$\text{Ni}_{45}\text{Co}_5\text{Mn}_{40}\text{Sn}_{10}$ prepared by arc melting the elemental materials Ni (99.999%), Mn (99.98%), Co (99.99%) and Sn (99.99%) under positive pressure of argon. The arc melting furnace was purged three times and a Ti getter was melted prior to melting each sample. To promote homogeneity, the ingot was melted and turned six times. Conversion from emu/g to emu/cm^3 was done with a density 8.0 g/cm^3 . All samples were weighed before and after melting and lost less than 1% by mass. The resulting buttons were homogenized in an evacuated and sealed quartz tube at $900 \text{ }^\circ\text{C}$ for 24 h, and quenched in water.

Magnetic measurements reported in Figure 1a,c,d were done on a Princeton Measurements micro vibrating sample magnetometer (VSM), calibrated using magnetite, at a heating/cooling rate of $6 \text{ }^\circ\text{C/min}$. The magnetic measurements reported in this paper were checked by cutting another sample from the same button and repeating the measurements. Differential scanning calorimetry (DSC) measurements were done on a Thermal Analyst, calibrated with indium, at a heating and cooling rate of $\pm 10 \text{ }^\circ\text{C/min}$. For the DSC measurements each sample was thinned and finely polished to ensure good thermal contact with the pan.

The experimental setup for the measurement of the induced emf is as shown in Figure 2. The permanent magnet having 6.35 cm diameter was used. The field at the pole is $\sim 0.5 \text{ T}$ and, near the place later occupied by the center of the sample, it is 0.2T. The coil has 2000 turns of copper wire having 0.13 mm diameter. The inner diameter of the coil is 1.9 cm and the outer diameter is 3.8 cm. A 10 k ohm resistance was connected in series with the device as indicated in Figure 2. A Keithley 2182 nanovoltmeter having an internal resistance of 10 G ohm was used to measure the voltage across the 10 k ohm resistance. The temperature was measured using a chromel alumel thermocouple, whose signal was measured in the second channel of the voltmeter. The thermocouple was placed just on the surface and below the sample, away from the direct flow of the heat gun. The nanovoltmeter was interfaced with the computer and the data were recorded at time intervals of 0.05 s. The sample was heated to above the transition temperature using a heat gun. The cooling occurred by natural conduction and convection.

Acknowledgements

We wish to thank Dave Hultman for numerous helpful suggestions. This work was supported by MURI W911NF-07-1-0410 administered by ARO. It also benefitted from the support of AFOSR GameChanger

program GRT00008581/RF60012388 and MURI N000140610530 ONR. We thank the Institute for Rock Magnetism, supported by NSF and UMN, for the use of its facilities for magnetic measurements.

Received: September 29, 2010

Revised: December 1, 2010

Published online: December 15, 2010

- [1] V. Srivastava, X. Chen, R. D. James, *Appl. Phys. Lett.* **2010**, *97*, 014101.
- [2] N. A. Spaldin, M. Fiebig, *Science* **2005**, *309*, 391.
- [3] T. Krenke, E. Duman, M. Acet, E. F. Wasserman, X. Moya, L. Mañosa, A. Planes, *Nat. Mater.* **2005**, *4*, 450.
- [4] T. Krenke, M. Acet, E. F. Wasserman, X. Moya, L. Mañosa, A. Planes, *Phys. Rev. B* **2005**, *72*, 014412.
- [5] R. Kainuma, Y. Imano, W. Ito, Y. Sutou, H. Morito, S. Okamoto, O. Kitakami, K. Oikawa, A. Fujita, T. Kanomata, K. Ishida, *Nature* **2006**, *439*, 957.
- [6] R. Kainuma, Y. Imano, W. Ito, H. Morito, Y. Sutou, K. Oikawa, A. Fujita, K. Ishida, S. Okamoto, O. Kitakami, T. Kanomata, *Appl. Phys. Lett.* **2006**, *88*, 192513.
- [7] T. Krenke, E. Duman, M. Acet, X. Moya, L. Mañosa, A. Planes, *J. Appl. Phys.* **2007**, *102*, 033903.
- [8] R. Ramesh, N. A. Spaldin, *Nat. Mater.* **2007**, *6*, 21.
- [9] H. E. Karaca, I. Karaman, B. Basaran, Y. Ren, Y. I. Chumlyakov, H. J. Maier, *Adv. Funct. Mater.* **2009**, *19*, 983.
- [10] K. Bhattacharya, R. D. James, *Science* **2005**, *307*, 53.
- [11] R. D. James, Z. Zhang, in *The Interplay of Magnetism and Structure in Functional Materials* (ed. L. Manosa, A. Planes, A. B. Saxena), Springer Series in Materials Science **2005**, *79*, 159.
- [12] E. Faran, D. Shilo, *Phys. Rev. Lett.* **2010**, *104*, 155501.
- [13] P. Krulevitch, A. P. Lee, P. B. Ramsey, J. C. Trevino, J. Hamilton, M. A. Northrup, *J. Microelectromech. Syst.* **1996**, *5*, 270.
- [14] K. Bhattacharya, S. Conti, G. Zanzotto, J. Zimmer, *Nature* **2004**, *428*, 55.
- [15] K. Bhattacharya, *Microstructure of Martensite*. Oxford University Press **2003**.
- [16] K. Gall, H. J. Maier, *Acta Mater.* **2002**, *50*, 4643.
- [17] T. Lim, D. McDowell, *J. Mech. Phys. Solids* **2002**, *50*, 651.
- [18] Z. Mounni, A. Van Herpen, P. Riberty, *Smart Mater. Struct.* **2005**, *14*, S287.
- [19] Z. Zhang, R. D. James, S. Müller, *Acta Mater.* **2009**, *57*, 4332. Invited overview.
- [20] R. Delville, S. Kasinathan, Z. Zhang, V. Humbeeck, R. D. James, D. Schryvers, *Phil. Mag.* **2010**, *90*, 177.
- [21] J. Cui, Y. S. Chu, O. Famodu, Y. Furuya, J. Hattrick-Simpers, R. D. James, A. Ludwig, S. Thienhaus, M. Wuttig, Z. Zhang, I. Takeuchi, *Nat. Mater.* **2009**, *5*, 286.
- [22] R. Zarnetta, R. Takahashi, M. L. Young, A. Savan, Y. Furuya, S. Thienhaus, B. Maaß, M. Rahim, J. Frenzel, H. Brunken, Y. S. Chu, V. Srivastava, R. D. James, I. Takeuchi, G. Eggeler, A. Ludwig, *Adv. Funct. Mater.* **2010**, *20*, 1917.
- [23] The size of the thermal hysteresis $A_s - M_f$ in several NiTiCuPd alloys having λ_2 extremely close to 1 is shown to be 0 within the experimental error of measurement of temperature. A_s , A_f , M_s , M_f are defined by the construction shown in Figure 1b.
- [24] Y. Song, V. Srivastava, K. Bhatti, R. D. James, *unpublished*.
- [25] A modest change of the diameter D of the specimen from 0.75 to 0.55 gives peaks of voltage vs. time near those measured in the experiment.
- [26] B. D. Cullity, *An Introduction to Magnetic Materials*, Addison-Wesley **1972**.
- [27] G. J. Snyder, E. S. Toberer, *Nature Materials* **2008**, *7*, 105.
- [28] D. T. Crane, J. W. LaGrandeur, F. Harris, L. E. Bell, *J. of Electronic Materials* **2009**, *38*, 1375.
- [29] Marlow Industries, Technical Data Sheet (preliminary), TG12-8 Thermoelectric Generator, DOC # 102-0344 REV F, 1–2.
- [30] In Ni₂MnGa the austenite is cubic with anisotropy constants K_1 near 4×10^4 ergs/cm³ and $K_2 = -9K_1/4$, while the martensite is uniaxial with $K_u = 2.45 \times 10^6$ erg/cm³, but the magnetization changes by a factor of only 7/8.
- [31] N. Tesla, US Patent 428,057, Pyromagneto-electric generator, **1887**.
- [32] W. S. Ginnell, J. L. McNichols, Jr., J. S. Cory, *Mechanical Engineering* **1979**, May Issue, 28.